

Sensitivity of Diffusion MRI to Perilesional Reactive Astrogliosis in Focal Ischemia

Rachel A. Weber^a, Clifford H. Chan^{b,c}, Xingju Nie^c, Emily Maggioncalda^a, Grace Valiulis^a,
Abigail Lauer^d, Edward S. Hui^e, Jens H. Jensen^{b,c*}, DeAnna L. Adkins^{a,c,f}

^aDepartment of Neuroscience, Medical University of South Carolina, Charleston, South Carolina, USA.

^bDepartment of Radiology and Radiological Science, Medical University of South Carolina, Charleston, South Carolina, USA.

^cCenter for Biomedical Imaging, Medical University of South Carolina, Charleston, South Carolina, USA.

^dDepartment of Public Health Science, Medical University of South Carolina, Charleston, South Carolina, USA.

^eDepartment of Diagnostic Radiology, Li Ka Shing Faculty of Medicine, The University of Hong Kong, Pokfulam, Hong Kong SAR, China.

^fDepartment of Health Science and Research, Medical University of South Carolina, Charleston, South Carolina, USA.

* Corresponding Author:

Jens H. Jensen, Ph.D.
Center for Biomedical Imaging
Department of Radiology and Radiological Science
Medical University of South Carolina
96 Jonathan Lucas Street, MSC 323
Charleston, SC 29425-0323
Tel: (843) 876-2467
Email: jense@musc.edu

Grant sponsors: National Institutes of Health

Grant numbers: R21NS085475 (NIH), T32GM008716 (NIH)

Word Count: 3607

ABSTRACT:

Reactive astrogliosis is a response to injury in the central nervous system that plays essential roles in inflammation and tissue repair. It is characterized by hypertrophy of astrocytes, alterations in astrocyte gene expression, and astrocyte proliferation. Reactive astrogliosis occurs in multiple neuropathologies, including stroke, traumatic brain injury, and Alzheimer's disease, and it has been proposed as a possible source of the changes in diffusion MRI (dMRI) metrics observed with these diseases. In this study, the sensitivity of dMRI to reactive astrogliosis is tested in an animal model of focal acute and subacute ischemia induced by the vasoconstricting peptide, endothelin-1. Reactive astrogliosis in perilesional cortex is quantified histologically by astrocyte surface density as determined with a glial fibrillary acidic protein (GFAP) antibody, while perilesional diffusion changes were measured *in vivo* with diffusional kurtosis imaging. We found substantial changes in the surface density of GFAP-positive astrocytes and modest changes in dMRI metrics in the perilesional motor cortex following stroke. Although there are time-point specific correlations between dMRI and histology measures, there is no definitive evidence for a causal relationship.

Keywords: astrogliosis; ischemia; perilesional; stereology; GFAP; diffusion; imaging; MRI

Abbreviations used: *DKI*, diffusional kurtosis imaging; *dMRI*, diffusion MRI; *ET-1*, endothelin-1; *FA*, fractional anisotropy; *GFAP*, glial fibrillary acidic protein; *IHC*, immunohistochemistry; *MAP2*, microtubule-associated protein 2; *MD*, mean diffusivity; *MK*, mean kurtosis; *ROI*, region of interest; *SMI-312*, pan-axonal neurofilament marker; *TBI*, traumatic brain injury.

INTRODUCTION

Diffusion MRI (dMRI) is commonly applied to investigate changes in brain tissue microstructure associated with neuropathologies such as stroke (1), traumatic brain injury (TBI) (2), and Alzheimer's disease (3). Nevertheless, the effects of specific microstructural features on diffusion properties measured with dMRI are poorly understood (4,5). In response to injury, a key process in brain tissue is reactive astrogliosis, which involves hypertrophy of astrocytes, alterations in astrocyte gene expression, and astrocyte proliferation (6). Reactive astrogliosis is an essential aspect of neuroinflammation and is associated with the preservation of blood brain barrier and tissue repair. As they are among the most numerous of glial cells, astrocytes provide important diffusion barriers, making it plausible that dMRI could be sensitive to reactive astrogliosis. Indeed, two prior studies of white matter injury have found correlations between markers of reactive astrogliosis and the axial diffusivity (7,8), while in gray matter associations between reactive astrogliosis and the fractional anisotropy (FA) and mean kurtosis (MK) have been observed for TBI (9,10). It has also been proposed that reactive astrogliosis may help to account for observed alterations in dMRI measures for stroke and Alzheimer's disease (11,12). However, some studies find no links between reactive astrogliosis and dMRI (13,14).

Here we examine the connections between dMRI and reactive astrogliosis occurring in a rat model of acute to subacute focal ischemia. It is well known that diffusion metrics are substantially altered within the core of ischemic lesions (1) and may also change significantly in perilesional regions (11,13,15). We utilize diffusional kurtosis imaging (DKI) (16-18) to quantify the diffusion properties and astrocyte surface density (19) to

quantify reactive astrogliosis. The DKI measurements are made in vivo just prior to sacrifice for histology. Astrocytes are visualized using standard immunohistochemistry (IHC) procedures and a glial fibrillary acidic protein (GFAP) antibody, a standard marker of reactive astrogliosis (20,21), and stereological methods (22) are applied to calculate the perilesional astrocyte surface density. Our primary goal is to test the sensitivity of diffusion metrics to reactive astrogliosis associated with acute and subacute focal ischemia.

METHODS

Animals

Long Evans male rats (n=67, 3-4 months old) received food and water *ad libitum* and were kept on a 12:12 hr light:dark cycle. Rats were randomly assigned to one of four groups that received endothelin-1 (ET-1) induced strokes and underwent dMRI scans at 3 hr (n=39), 1 day (n=29), 3 days (n=19), and 7 days (n=10) post-injury. Shortly after these scans, a subset of animals were sacrificed for IHC at 3 hr (n=10), 1 day (n=10), 3 days (n=9), and 7 days (n=10). Animals that failed to exhibit a lesion at the 3 hr post-injury time point were not considered in the data analysis (n=9). For comparison, this study included sham animals (n=19) without strokes that also underwent dMRI and were sacrificed for histology. All work was done in accordance with the Medical University of South Carolina Animal Care and Use Committee guidelines.

Surgical Procedures

Animals were anesthetized with a cocktail of ketamine (110 mg/kg) and xylazine (70 mg/kg). Unilateral ischemic lesions were induced via infusion of ET-1 (American Peptide, Inc) into layer V of the left forelimb area of the sensorimotor cortex through two

holes drilled at 1.0 mm posterior and 2.0 mm anterior and 4.1 mm lateral to bregma (21). A total of 1.2 μl of ET-1 (0.2 $\mu\text{g}/\mu\text{l}$ in sterile saline) was injected into each hole via a Hamilton syringe (lowered to -2.5 mm DV), at a rate of 0.6 $\mu\text{l}/\text{min}$. After the final application of ET-1, the brain was left undisturbed for 5 min and then the holes were covered with gel film and ultraviolet-cured dental acrylic (SDI Limited Inc.). Sham animals were anesthetized, received a midline incision and were sutured.

Diffusion Magnetic Resonance Imaging

dMRI scans were acquired at pre-injury and at 3 hr, 1 day, 3 days, and 7 days post-injury, using a 7T/30 Bruker BioSpec (Billerica, MA) animal scanner. Animals were anesthetized with isoflurane/air (4-5% for induction/1-3% for maintenance) for all dMRI scans. A standard DKI (18) protocol was utilized consisting of a two-shot spin-echo echo planar imaging diffusion sequence with 30 diffusion encoding directions and 5 b-values (0, 500, 1000, 1500, 2000 s/mm^2). Other imaging parameters were: TR/TE = 4750/32.5 ms, field of view = 30 \times 30 mm^2 , matrix = 128 \times 128, in-plane resolution = 0.23 \times 0.23 mm^2 , slice thickness = 1.0 mm, diffusion gradient pulse duration = 5 ms, diffusion time = 18 ms, and number of excitations = 2. A total of 19 axial slices with no interslice gap were collected.

For quantification of diffusion parameters, the dMRI data was post-processed with the Diffusional Kurtosis Estimator (23) software (<https://www.nitrc.org/projects/dke/>), which generated parametric maps of the mean diffusivity (MD), FA, and MK. Directional diffusion metrics, such as the axial diffusivity and kurtosis, were not employed, since this study focuses on cortical gray matter regions for which the directional metrics provide

relatively little additional information beyond that contained in the mean metrics and FA, due to the low diffusion anisotropy of gray matter.

Regions of interest (ROIs) were drawn manually in the lesion core and perilesional motor cortex. All ROIs were inspected for consistency by a single investigator (R.A.W.). For the 3 hr, 1 day, and 3 day time points, the lesion core was defined as the distinctly hyperintense voxels on the direction-averaged dMRI images with $b = 2000 \text{ s/mm}^2$. As this was often not feasible for animals at 7 days due to tissue degradation, lesion core ROIs were not defined at this time point. Nonetheless, perilesional ROIs were defined at 7 days so as to be in similar anatomical location as with the earlier time points. The pre-operative ROIs were chosen to be similar to the ROIs defined at 3 hr, since all the stroke animals were imaged then. All ROIs spanned 3 consecutive slices that encompass the site of injury, the primary motor cortex. Examples of ROIs for a single slice in one animal are shown in Figure 1.

Tissue Processing

Following MRI scans, subsets of animals at 3 hr, 1 day, 3 days, or 7 days post-injury were deeply anesthetized with pentobarbital (Euthasol, 100-150mg/kg, IP) and were intracardial perfused with 0.1M phosphate-buffer and 4% paraformaldehyde. Six serial rostral to caudal sets of 50 μm coronal sections were produced using a vibratome and stored in cryoprotectant. Three sets of sections were processed for IHC to ascertain post-injury morphological changes in the surface density of astrocytes, dendrites, and axons in the perilesional motor cortex.

Briefly, as described previously (11,21), free-floating sections were processed for IHC. Tissue was incubated for 48 hr in one of the following primary antibodies: GFAP for astrocytes (1:800 rabbit polyclonal; Dako), microtubule protein 2 (MAP2) for dendrites (1:500 mouse monoclonal; Sigma-Aldrich), and for axons, pan-axonal neurofilament marker (SMI-312; 1:1000 mouse monoclonal; BioLegend). Following primary incubation, sections were rinsed and incubated for 2 hr in secondary antibody at a dilution of 1:200 (horse anti-mouse for MAP2 and SMI-312; goat anti-rabbit for GFAP). Sections were incubated in peroxidase-linked avidin-biotin complex (ABC kit) for 2 hr. Immunoreactivity was visualized using 3,3' diaminobenzidine with nickel ammonium sulfate intensification. All animals were included in each batch of IHC processing and each batch included negative control sections without primary antibody.

Microstructure Quantification

The cycloid grid intersection method (22) was used to determine surface density for the GFAP, MAP2 and SMI-312 immuno-reactive processes. For each antibody, we sampled tissue that was represented in three adjacent MRI slices that included the forelimb area of the sensorimotor cortex. Data were obtained in three adjacent coronal sections (~600 μm apart) which included perilesional motor cortex (i.e., between approximately +1.2 and -0.26 mm anterior/posterior relative to bregma) (24). Using ImageJ (National Institute of Mental Health, Bethesda, MD), cycloid arcs were overlaid on light microscopic images, taken at 100 \times oil immersion (final magnification=1,400 \times), of four sample regions, two adjacent sets (~250 μm) in layers II/III and two sets in layer V beginning at approximately 250 μm medial to the lesion core (towards midline), for 3 sections. Each

immuno-reactive process that crossed an arc was counted. The surface density was calculated using the formula $S_v = 2(I/L)$, where S_v is the surface density, I is the total number of intersections and L is the sum of the cycloid arc lengths. Surface densities were not obtained for the lesion core as tissue was not viable or our antibodies did not react in the core at 72 hr and later.

Statistical Analysis

Linear mixed models were used to analyze dMRI metrics with injury group and time point, and their interaction as covariates. Normality assumptions were assessed prior to running the models and outliers were removed when necessary. A random intercept was used in the model to account for replicates. Post-hoc pairwise comparisons used a Scheffe's adjustment. Analysis of variance (ANOVA) models were used to look for a relationship between histology measures by group and injury, as well as their interaction. A significance level of 0.05 was used for all other outcomes. Due to a small sample size at each time point, when examining dMRI and histology measures Spearman correlations with a corrected p-value were used. Correlations with a strong correlation coefficient ($r > 0.7$) were deemed relevant. Bonferroni adjustments were made for multiple comparisons in the correlations to account for the number of time points being compared.

RESULTS

Representative maps of MD, FA, and MK for a single slice from one animal sacrificed at 7 days are shown in **Figure 1**. Substantial changes within the lesion core are apparent for all three metrics, which are consistent with ischemia (**Fig. 2A-C**). In the lesion core, there was a significant time by injury interaction ($F_{149}=44.7$, $p < 0.001$) and a

significant decrease in MD at 3 hours ($p < 0.001$) and 24 hours ($p < 0.001$) compared to sham animals and pre-operative levels, which renormalized by day 3 post-injury (**Fig. 2A**). This result is consistent with previous data in the field (1,11,25-27). Additionally, there was also a significant time by injury interaction with MK ($F_{156}=39.31$, $p < 0.001$), and MK remained elevated at all time points: 3 hr ($p < 0.001$), 24 hr ($p < 0.001$), and 72 hr ($p < 0.001$) which is consistent with previous reports (**Fig. 2B**; 1,11,25-27). Lastly, there was a significant interaction of time by injury in FA ($F_{134}=17.83$, $p < 0.001$) and FA was significantly reduced in the lesion core at 24 hr ($p < 0.001$) and 72 hr ($p < 0.001$) post-injury (**Fig. 2C**).

We examined the same metrics (MD, MK, and FA) in the perilesional motor cortex (**Fig. 2D-E**), which has been less well studied. There was a significant injury by time interaction in MD in the perilesional cortex ($F_{133}=5.96$, $p < 0.001$) and MD was significantly decreased at 3 hr ($p < 0.001$) post-injury compared to sham animals and pre-operative levels (**Fig. 2D**). There was not a significant interaction of injury and time in MK, only a significant effect of time ($F_{151}=4.781$, $p=0.001$). There was a slight increase in MK at 3 hr ($p=0.016$) compared to pre-operative levels (**Fig. 2E**). There was a significant interaction of injury and time ($F_{146}=7.222$, $p < 0.001$) in perilesional FA which was elevated 3 hr ($p < 0.001$) and 24 hr ($p=0.006$) post-injury compared to pre-operative levels (**Fig. 2F**). These data indicate that not only are dMRI metrics sensitive to differences in the lesion core, but also are able to detect changes in the perilesional area of the motor cortex, which undergoes ischemia-induced, time-dependent biochemical and structural changes (28).

Lastly, we examined the surface density of glia and dendrite processes and axons in the perilesional cortex (**Fig. 3**). It should be noted that by post-injury Day 3, tissue in the lesion core is likely not viable and does not react to the antibodies used in this study (**Fig.**

3A); thus, we focused on astrocytic (GFAP positive cells) and neural (dendrites and axons) structural changes in perilesional cortex and related these to dMRI metrics. There was a significant interaction of time and injury ($F_{49}=8.03$, $p<0.001$) and significant increases in the density of immuno-positive GFAP processes at 3 days ($p=0.005$) and 7 days ($p<0.001$) post-injury compared to sham animals (**Fig. 3B**). As seen in **Figure 3C**, there was a significant and strong positive correlation at 24 hr between GFAP positive processes and perilesional FA ($r=0.85$, $p=0.001$). There was also a strong and significant correlation between GFAP-positive processes and perilesional MD on post-injury day 7 ($r=0.78$, $p=0.01$; **Fig. 3D**). These data suggest that astrocytes may play a role in the early increase in FA levels after stroke and in the return of MD to pre-stroke levels, as previously reported (11). However, as discussed in more detail below, these data more strongly suggest that dMRI is likely reflecting other morphological and structural changes not measured in this study, given that neither FA, MD nor MK changed in synch with the relatively large increase in GFAP positive processes that occurred over the hours and days after ischemia.

There was not a significant interaction of time and injury in perilesional density of axon (SMI-312-positive) or dendritic (MAP2-positive) processes (**Fig. 4A&B**). However, at 24 hr after injury, there was a strong and positive correlation between the density of SMI-312-positive axons and perilesional MD ($r=0.78$, $p=0.008$; **Fig. 4C**). Our data suggest that changes in axonal and astrocyte density might be involved in some of the changes in MD and FA. It is possible that since we examined a fairly large number of comparisons (3 antibodies X 3 dMRI X 4 time-points = 36) these correlations are statistical anomalies. However, given that we only considered r-values over 0.7 to be relevant and corrected for multiple-comparisons, these data potentially do reflect real associations between alterations

in water diffusion as measured by MD, MK and FA and cellular structure or function changes.

DISCUSSION

Consistent with prior studies of acute to subacute stroke in animal models (11,26,27), we observe that in the core of the lesion tissue MD initially drops following ischemic injury and then returns to near normal values by 3 days and that MK markedly increases following ischemia and remains elevated out to 3 days. We also observe that following ischemic damage the FA value is significantly below the pre-injury and sham levels at 1 and 3 days post-stroke. In perilesional cortex, we find a decrease in the MD at 3 hr and an increase in FA at 3 hr and 24 hr compared to pre-operative levels and sham animals. This MD drop is consistent with a similar prior study by our group (11). However, this prior study also observed a small but significant increase in the MK at 3 days, whereas we did not replicate this in our current study. This may be, in part, due to smaller lesions examined by ROI analysis in the present study (482 ± 58 voxels) compared to our early report (1188 ± 237 voxels), and thus perilesional cortex MK responses could be less robust (11).

There was a substantial degree of reactive astrogliosis, as measured by GFAP+positive immuno-reactivate processes, in the perilesional cortex at 3 and 7 days post-injury, with a more than threefold increase at 7 days in comparison to the baseline values from the sham animals. In our prior study (11), a statistically significant correlation between the surface density for GFAP and the perilesional MD at 3 days is reported, but

this finding is not reproduced here ($r=0.09$). We do however show a significant correlation between GFAP and perilesional MD at 7 days in our current analysis. Again, the later time point correlation may be due to the fact that our lesions were smaller in the present study, which may have delayed some aspects of the injury response. Astrocyte density correlated as well with perilesional FA 24 hr after stroke, but not at any other time points. In other models, including traumatic brain injury, GFAP intensity has also been associated with FA levels (9).

In contrast with the GFAP measurements, the perilesional surface densities for dendrites (MAP2) and axons (SMI-312) varied little across the time points, consistent with minimal disruption in the structural density of these microstructural components within the perilesional cortex. We did detect a significant correlation between axons and perilesional FA early after stroke, even though there was a non-significant reduction in axonal processes (**Fig. 4A&C**). FA may be detecting axonal degeneration and axonal demyelination, which has been proposed in other models of injury (9). Previous research has shown a link between axonal changes and FA in white matter tracts (9,30,31). Further studies are needed to determine this possible relationship.

Astrogliosis is a common feature of CNS injury and disease that produces a variety of cellular, molecular, structural and functional changes that, depending on the severity of insult, can result in progressive hypertrophy and in severe cases glia scar formation and proliferation. As noted by Sofroniew and Vinters (6), GFAP antibodies can be used as a sensitive and reliable marker that labels most CNS injury-induced reactive astrogliosis. GFAP antibodies also do not necessarily react to all astrocytes in healthy tissue nor does it

reveal all the fine distal processes. Further, mild to moderate reactive astrogliosis often leads to only negligible astrocyte proliferation (6). Thus, the observed increase in astrocyte surface density changes in this study likely does not reflect astrocyte proliferation but instead an upregulation of injury-induced GFAP astrocytes undergoing lesion induced morphological and functional changes. It is possible that a more severe reactive astrogliosis, with astrocyte proliferation and glial scar formation, would be more robustly detectable with dMRI. For a rat model of TBI, Zhuo and coworkers (10) found evidence linking increased MK with increased GFAP immunoreactivity in gray matter. Similarly, Budde and coworkers (9) found that GFAP expression in cortical gray matter had a significant positive relationship with FA for TBI. Other studies that have attempted to link reactive astrogliosis with diffusion measures report both positive (7,8) and negative results (13,14).

Our study possesses several limitations that should be taken into consideration when interpreting the results. The majority of studies that attempt to find causal links between dMRI and histological measures have used correlations between the two, as we have done, but as the old adage states—correlations do not determine causality. Future studies would benefit from using conditional knockout or knockin animals to help determine the effects of altering the expression of different cell types or their structure on dMRI metrics. We examined three different cell types using IHC; however many more factors could be contributing to changes detected by dMRI. For example, edema, microglia activation, inflammation, and cellular apoptosis might also alter dMRI metrics following stroke (9,13,32).

One important limitation of this study is that GFAP is not necessarily strongly expressed in all astrocytes, and so our measured astrocyte surface densities likely only reflect a subset of these cells and should be interpreted accordingly (6). Nonetheless, GFAP expression is regarded as a standard marker for reactive astrogliosis (6,20,21), and our surface densities may therefore be considered as valid measures of reactive astrogliosis severity. Another limitation is possible displacement of the perilesional tissue due to tissue degradation within the lesion core over the course of the experiment, which could confound the positioning of our perilesional ROIs and contribute to the variability of our measurements. For this reason, all ROIs were inspected by a single investigator (R.A.W.) for consistency.

CONCLUSION

MD, FA, and MK in the perilesional cortex of focal ischemic injury show minimal changes at 1, 3 and 7 days post-injury despite monotonic increase in reactive astrogliosis, to over threefold above baseline values at 7 days post-injury. We also found a positive correlation between increased GFAP-immunoreactivity in the perilesional gray matter and FA acutely (24 h) and MD subacutely (7 days) following focal ischemia. However, the dMRI metrics do not correlate across all post-injury time points with GFAP positive astrocytes and thus these correlations may indicate a yet unidentified driver of diffusional changes of which astrogliosis could be involved or related to, but not necessarily the main cause.

ACKNOWLEDGEMENTS

Technical assistance was provided by Elyse Clayton and Zac Manahan. We are grateful to Maria F. Falangola for helpful discussions. This work was supported, in part, by the National Institutes of Health research grants R21NS085475 (to J. Jensen and D. Adkins), P20 GM109040 (DLA) and T32GM008716 (to P. Halushka).

REFERENCES

1. Fung SH, Roccatagliata L, Gonzalez RG, Schaefer PW. MR diffusion imaging in ischemic stroke. *Neuroimaging Clin. N. Am.* 2011; 21(2): 345-377. doi: 10.1016/j.nic.2011.03.001.
2. Delouche A, Attyé A, Heck O, Grand S, Kastler A, Lamalle L, Renard F, Krainik A. Diffusion MRI: Pitfalls, literature review and future directions of research in mild traumatic brain injury. *Eur. J. Radiol.* 2016; 85(1): 25-30. doi: 10.1016/j.ejrad.2015.11.004.
3. Goveas J, O'Dwyer L, Mascalchi M, Cosottini M, Diciotti S, De Santis S, Passamonti L, Tessa C, Toschi N, Giannelli M. Diffusion-MRI in neurodegenerative disorders. *Magn. Reson. Imaging.* 2015; 33(7): 853-876. doi: 10.1016/j.mri.2015.04.006.
4. Jones DK, Knösche TR, Turner R. White matter integrity, fiber count, and other fallacies: the do's and don'ts of diffusion MRI. *Neuroimage.* 2013; 73: 239-254. doi: 10.1016/j.neuroimage.2012.06.081.
5. Jelescu IO, Veraart J, Fieremans E, Novikov DS. Degeneracy in model parameter estimation for multi-compartmental diffusion in neuronal tissue. *NMR Biomed.* 2016; 29(1): 33-47. doi: 10.1002/nbm.3450.
6. Sofroniew MV, Vinters HV. Astrocytes: biology and pathology. *Acta Neuropathol.* 2010; 119(1): 7-35. doi: 10.1007/s00401-009-0619-8.
7. Wang S, Wu EX, Qiu D, Leung LH, Lau HF, Khong PL. Longitudinal diffusion tensor magnetic resonance imaging study of radiation-induced white matter

- damage in a rat model. *Cancer Res.* 2009; 69(3): 1190-1198. doi: 10.1158/0008-5472.CAN-08-2661.
8. Falangola MF, Guilfoyle DN, Tabesh A, Hui ES, Nie X, Jensen JH, Gerum SV, Hu C, LaFrancois J, Collins HR, Helpert JA. Histological correlation of diffusional kurtosis and white matter modeling metrics in cuprizone-induced corpus callosum demyelination. *NMR Biomed.* 2014; 27(8): 948-957. doi: 10.1002/nbm.3140.
 9. Budde MD, Janes L, Gold E, Turtzo LC, Frank JA. The contribution of gliosis to diffusion tensor anisotropy and tractography following traumatic brain injury: validation in the rat using Fourier analysis of stained tissue sections. *Brain.* 2011; 134(Pt 8): 2248-2260. doi: 10.1093/brain/awr161.
 10. Zhuo J, Xu S, Proctor JL, Mullins RJ, Simon JZ, Fiskum G, Gullapalli RP. Diffusion kurtosis as an in vivo imaging marker for reactive astrogliosis in traumatic brain injury. *Neuroimage.* 2012; 59(1): 467-477. doi: 10.1016/j.neuroimage.2011.07.050.
 11. Weber RA, Hui ES, Jensen JH, Nie X, Falangola MF, Helpert JA, Adkins DL. Diffusional kurtosis and diffusion tensor imaging reveal different time-sensitive stroke-induced microstructural changes. *Stroke.* 2015; 46(2): 545-550. doi: 10.1161/STROKEAHA.114.006782.
 12. Fieremans E, Benitez A, Jensen JH, Falangola MF, Tabesh A, Deardorff RL, Spampinato MV, Babb JS, Novikov DS, Ferris SH, Helpert JA. Novel white matter tract integrity metrics sensitive to Alzheimer disease progression. *AJNR Am. J. Neuroradiol.* 2013;34(11):2105-2112. doi: 10.3174/ajnr.A3553.

13. Umesh Rudrapatna S, Wieloch T, Beirup K, Ruscher K, Mol W, Yanev P, Leemans A, van der Toorn A, Dijkhuizen RM. Can diffusion kurtosis imaging improve the sensitivity and specificity of detecting microstructural alterations in brain tissue chronically after experimental stroke? Comparisons with diffusion tensor imaging and histology. *Neuroimage*. 2014; 97: 363-373. doi: 10.1016/j.neuroimage.2014.04.013.
14. Guglielmetti C, Veraart J, Roelant E, Mai Z, Daans J, Van Audekerke J, Naeyaert M, Vanhoutte G, Delgado Y Palacios R, Praet J, Fieremans E, Ponsaerts P, Sijbers J, Van der Linden A, Verhoye M. Diffusion kurtosis imaging probes cortical alterations and white matter pathology following cuprizone induced demyelination and spontaneous remyelination. *Neuroimage*. 2016; 125: 363-377. doi: 10.1016/j.neuroimage.2015.10.052.
15. Li L, Jiang Q, Ding G, Zhang L, Zhang ZG, Li Q, Panda S, Kapke A, Lu M, Ewing JR, Chopp M. MRI identification of white matter reorganization enhanced by erythropoietin treatment in a rat model of focal ischemia. *Stroke*. 2009; 40(3): 936-941. doi: 10.1161/STROKEAHA.108.527713.
16. Jensen JH, Helpert JA, Ramani A, Lu H, Kaczynski K. Diffusional kurtosis imaging: the quantification of non-Gaussian water diffusion by means of magnetic resonance imaging. *Magn. Reson. Med*. 2005; 53(6): 1432-1440.

17. Lu H, Jensen JH, Ramani A, Helpert JA. Three-dimensional characterization of non-Gaussian water diffusion in humans using diffusion kurtosis imaging. *NMR Biomed.* 2006; 19(2): 236-247.
18. Jensen JH, Helpert JA. MRI quantification of non-Gaussian water diffusion by kurtosis analysis. *NMR Biomed.* 2010; 23(7): 698-710. doi: 10.1002/nbm.1518.
19. Hawrylak N, Boone D, Salm AK. The surface density of glial fibrillary acidic protein immunopositive astrocytic processes in the rat supraoptic nucleus is reversibly altered by dehydration and rehydration. *Neurosci. Lett.* 1999; 277(1): 57-60.
20. Eng LF, Ghirnikar RS, Lee YL. Glial fibrillary acidic protein: GFAP-thirty-one years (1969-2000). *Neurochem. Res.* 2000; 25(9-10): 1439-1451.
21. Adkins DL, Voorhies AC, Jones TA. Behavioral and neuroplastic effects of focal endothelin-1 induced sensorimotor cortex lesions. *Neuroscience.* 2004; 128(3): 473-486.
22. Baddeley AJ, Gundersen HJ, Cruz-Orive LM. Estimation of surface area from vertical sections. *J. Microsc.* 1986; 142(Pt 3): 259-276.
23. Tabesh A, Jensen JH, Ardekani BA, Helpert JA. Estimation of tensors and tensor-derived measures in diffusional kurtosis imaging. *Magn. Reson. Med.* 2011; 65(3): 823-836. doi: 10.1002/mrm.22655.
24. Paxinos G, Watson C. *The rat atlas in stereotaxic coordinates.* New York: Academic, 1998.
25. Jensen JH, Falangola MF, Hu C, Tabesh A, Rapalino O, Lo C, Helpert JA. Preliminary observations of increased diffusional kurtosis in human brain

- following recent cerebral infarction. *NMR Biomed.* 2011; 24(5): 452-457. doi: 10.1002/nbm.1610.
26. Hui ES, Du F, Huang S, Shen Q, Duong TQ. Spatiotemporal dynamics of diffusional kurtosis, mean diffusivity and perfusion changes in experimental stroke. *Brain Res.* 2012; 1451: 100-109. doi: 10.1016/j.brainres.2012.02.044.
 27. Zhang S, Yao Y, Shi J, Tang X, Zhao L, Zhu W. The temporal evolution of diffusional kurtosis imaging in an experimental middle cerebral artery occlusion (MCAO) model. *Magn. Reson. Imaging.* 2016; 34(7): 889-895. doi: 10.1016/j.mri.2016.04.016.
 28. Carmichael ST, Kathirvelu B, Schweppe CA, Nie EH. Molecular, cellular, and functional events in axonal sprouting after stroke. *Exp Neurol.* 2016 ; 16 :30029-2. doi: 10.1016/j.expneurol.2016.02.007.
 29. Manley GT, Fujimura M, Ma T, Noshita N, Filiz F, Bollen AW, et al. Aquaporin-4 deletion in mice reduces brain edema after acute water intoxication and ischemic stroke. *Nat Med.* 2000 ;6 :159–163. doi: 10.1038/72256.
 30. Jiang Q, Zhang ZG, Chopp M. MRI of stroke recovery. *Stroke.* 2010 ;41 :410–414. doi: 10.1161/STROKEAHA.109.568048.
 31. Liu Z, Li Y, Zhang L, Xin H, Cui Y, Hanson LR, et al. Subacute intranasal administration of tissue plasminogen activator increases functional recovery and axonal remodeling after stroke in rats. *Neurobiol Dis.* 2012 ;45 :804–809. doi: 10.1016/j.nbd.2011.11.004.

32. Moseley ME, Cohen Y, Mintorovitch J, Chileuitt L, Shimizu H, Kucharczyk J, et al. Early detection of regional cerebral ischemia in cats: comparison of diffusion- and T2-weighted MRI and spectroscopy. *Magn Reson Med.* 1990 ;14 :330–346.

FIGURE CAPTIONS

Figure 1: Representative ROIs used for the quantification of diffusion metrics superimposed on dMRI images with $b = 0$ from all time points for one animal (first row). An ischemic lesion was induced in the cortex with ET-1. The red ROIs are the lesion core and the blue ROIs represent perilesional motor cortex. The lesion core ROIs were manually drawn based on the direction-averaged dMRI images with $b = 2000 \text{ s/mm}^2$ (second row). Lesion core ROIs were not defined for the 7 day time point due to difficulty in identifying the core. For the pre-injury time point, the lesion core ROI was chosen to be similar to that for the 3 hr time point. Parametric maps of the MD (third row) show a drop in the core for the 3 hr and 1 day time points, while the FA of the core (fourth row) is low for all post-injury time points. The MK of the core (fifth row) is, in contrast, elevated following ischemia.

Figure 2: Time courses for MD, FA, and MK in both the lesion core and the perilesional cortex. Dashed lines indicate sham levels. In the lesion core we found decreases in MD at 3 hr and 24 hr post-injury (**A.**), increases in MK at 3 hr, 24 hr, and 72 hr after injury (**B.**), and a decrease in FA at 24 hr and 72 hr after stroke (**C.**). These results are consistent with previous reports. In the perilesional cortex we found a decrease in MD at 3 hrs (**D.**) and an increase in FA at 3 hr and 24 hr post-injury (**F.**). There was not any change in perilesional MK following stroke in our model (**E.**). Perilesional cortex has been examined less post-injury.

Figure 3: A. The 7 day $b=0$ dMRI image with the perilesional ROI compared to a GFAP-stained section of sampled tissue (scale bar=0.5mm) to compare regions of sampling

between dMRI and histology. The sampled region of GFAP is enlarged to a 100x image to demonstrate our staining levels (scale bar=50um). Lastly, to illustrate our quantification technique we overlaid our cycloid grid arc filter used for counting on an enlarged section of GFAP stained tissue (scale bar=50um). **B.** Immuno-reactive GFAP staining in the perilesional cortex and the dashed line indicates sham levels. We observed an increase in GFAP at 3 days and 7 days post-injury. **C.** At 24 hr post-injury, we found a correlation between perilesional FA and GFAP, and at 7 days we found a correlation between perilesional MD and GFAP (**D.**).

Figure 4: **A.** Levels of immune-reactive SMI-312 in the perilesional cortex revealed no differences across time points after stroke. **B.** There was not a significant difference in MAP2 processes over the acute time after stroke, dashed line represents sham animals. Lastly, at 24 hr after stroke SMI-312 was significantly correlated with perilesional MD (**C.**).

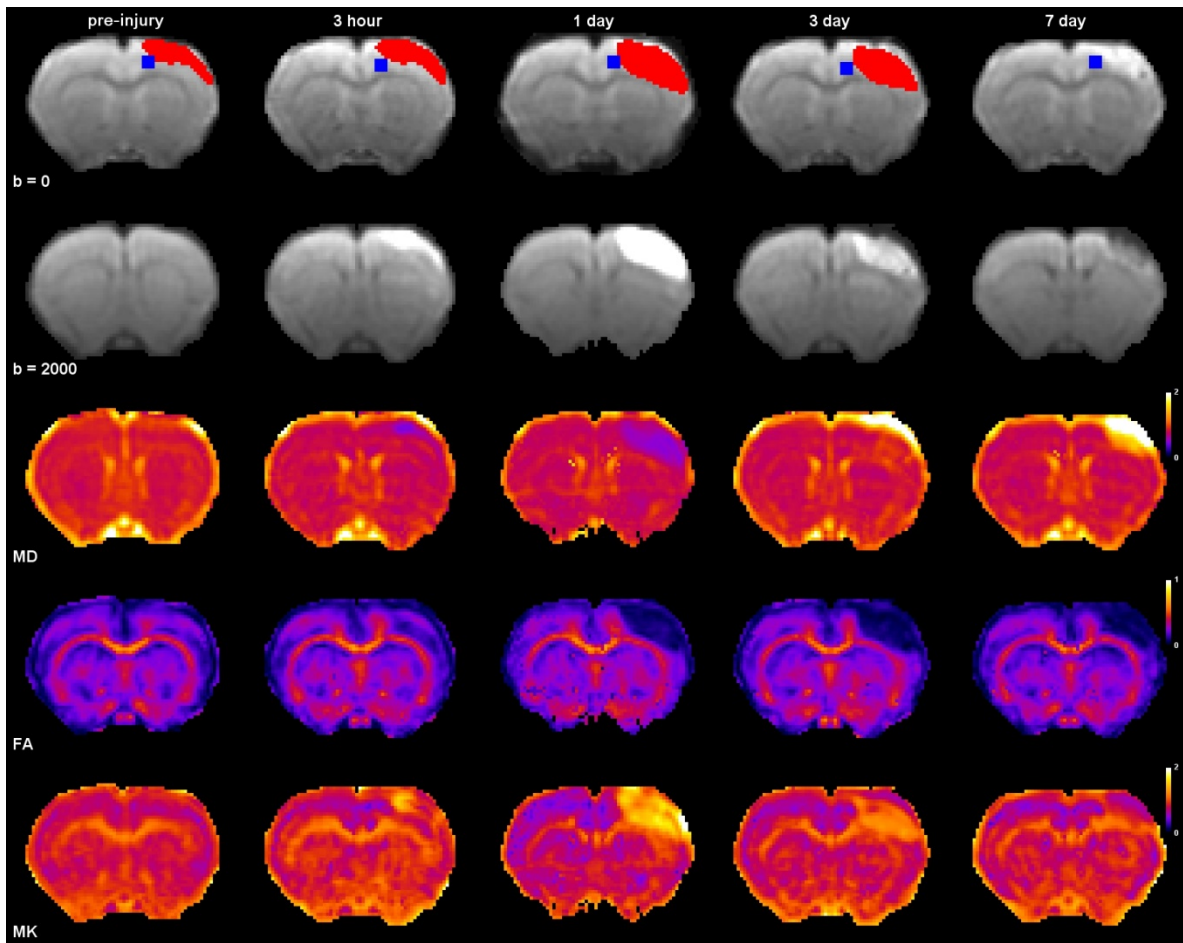


Figure 1

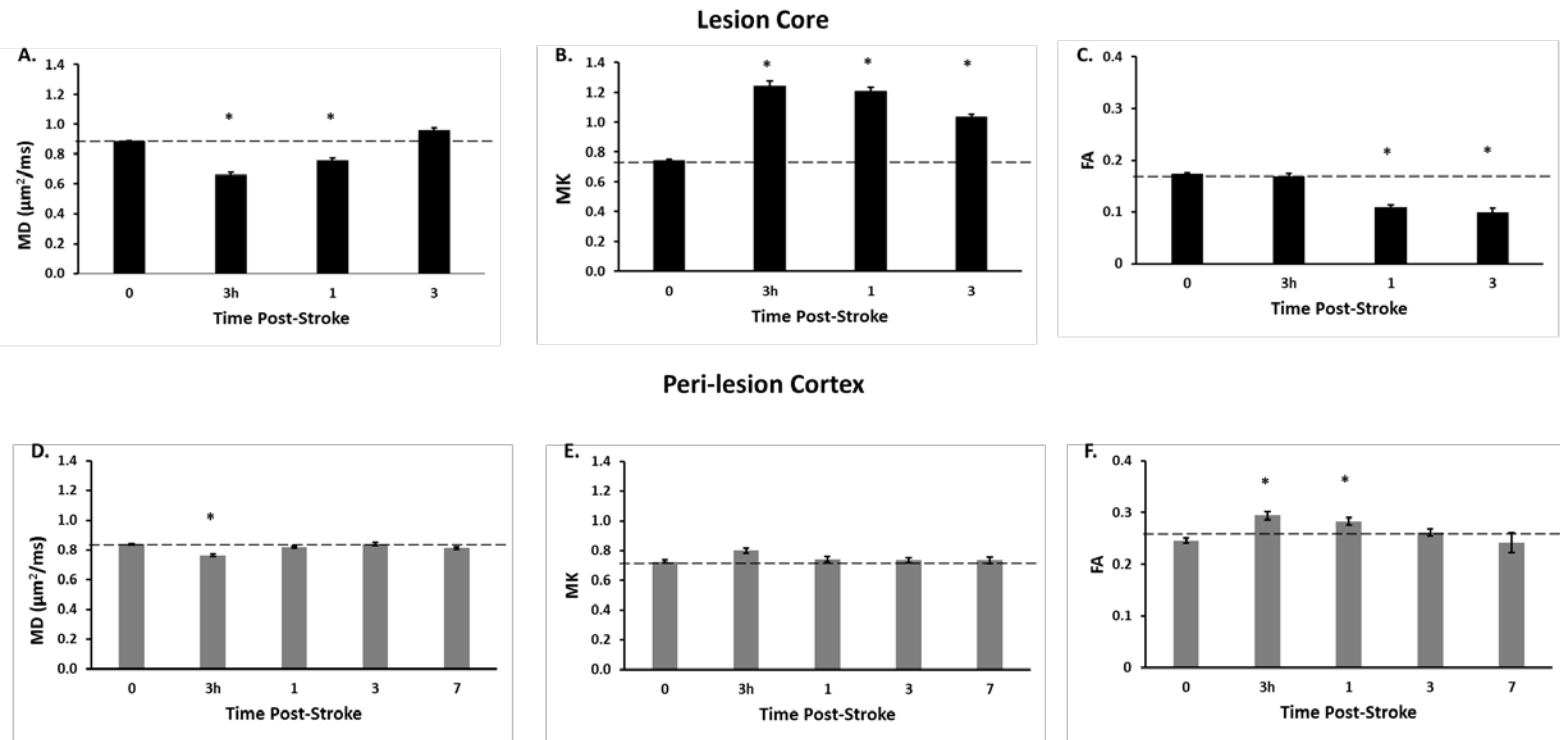


Figure 2

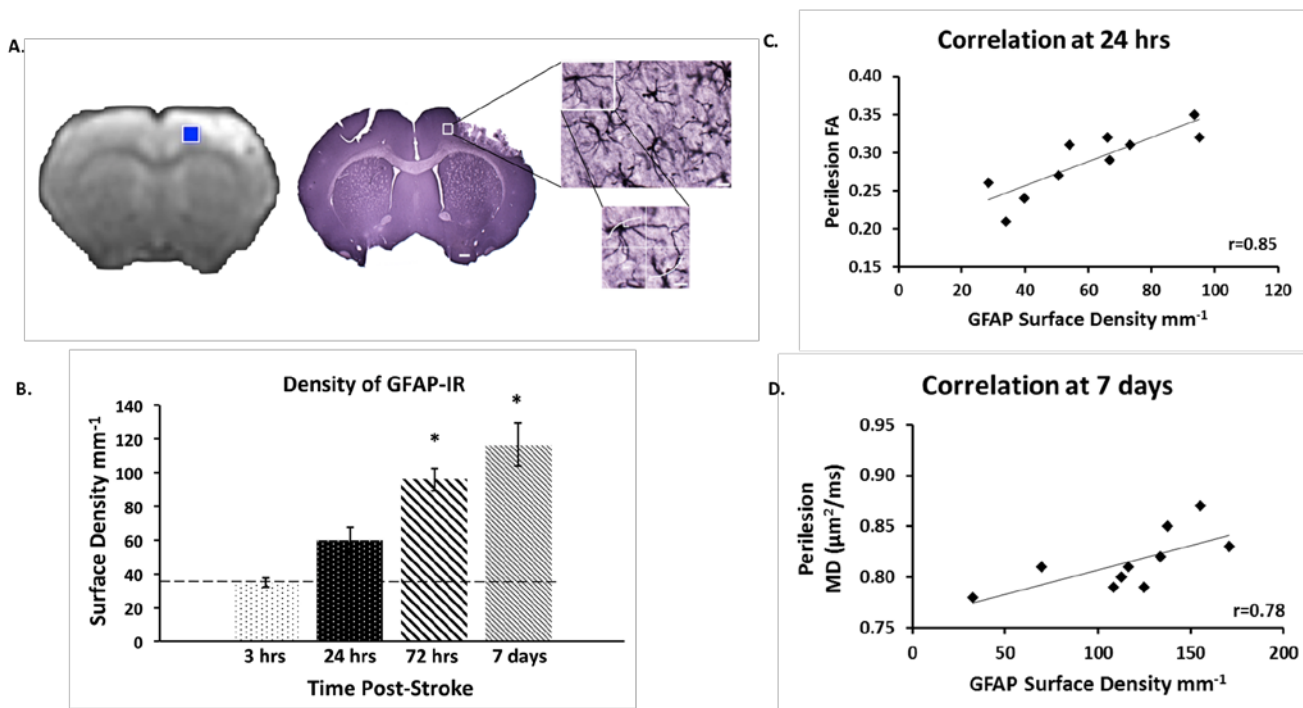


Figure 3

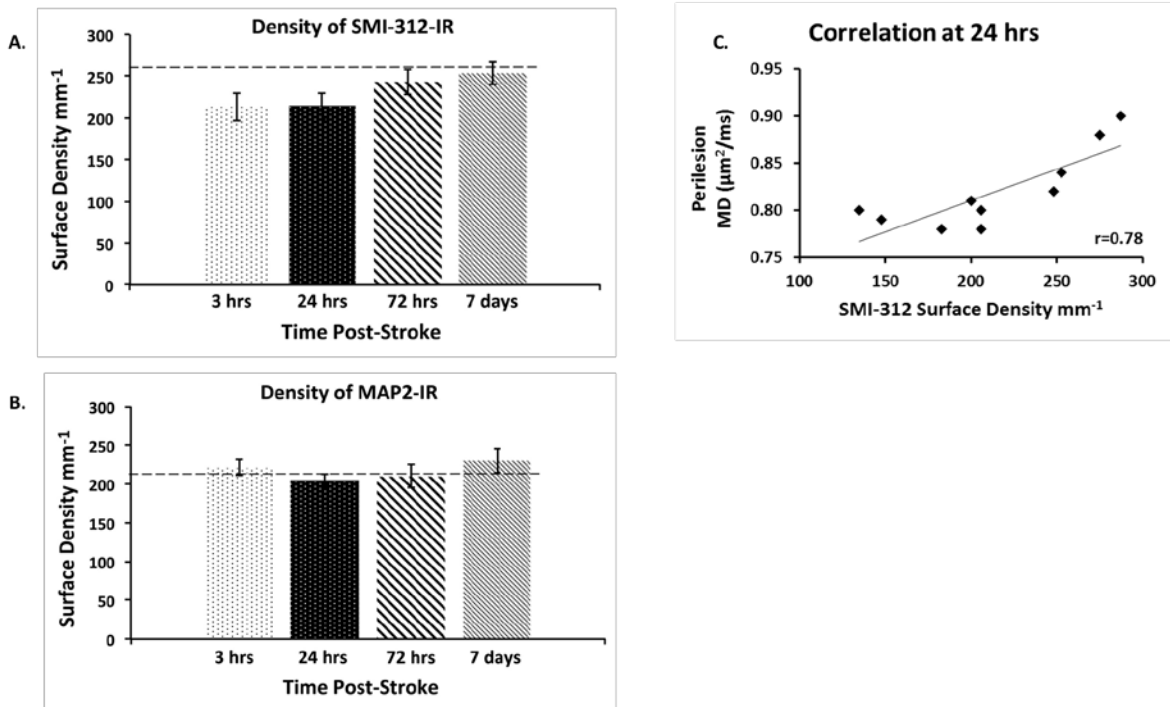


Figure 4